NUMERICAL SOLUTIONS OF 3D TRANSONIC VISCOUS FLOWS BY USING UPWIND-RELAXATION SWEEPING ALGORITHM

Ge-Cheng Zha* and E. Bilgen

Dept. of Mechanical Engineering, Ecole Polytechnique,
University of Montreal, P.O. Box 6079, St. A,
Montreal, H3C 3A7, Canada

Abstract

Upwind Relaxation-Sweeping (URS) algorithm is employed to solve the 3D Navier-Stoke equations to study the flow field for a three-dimensional non-axisymmetric transonic nozzle. Oblique shock waves and reflections are captured with the interaction with the wall boundary layers. The computational results agree favorably with the experiment.

Introduction

Multiengined, highly manoeuvrable jet aircraft must operate efficiently over a wide range of power settings and Mach numbers. Such aircraft requires a propulsion exhaust-nozzle system with a variable geometry for high performance. The application of an axisymmetric nozzle system to a typical multiengined jet configuration produces certain aircraft performance penalties, such as high aft-end drag. Investigations of the effects of nozzle design on twin-engine jet aircraft performance show that a high level of nozzle performance, without considerable aft-end drag, results from use of the nonaxisymmetric nozzle concept. The non-axisymmetric nozzle geometry is more efficiently integrated into the airframe eliminating the boat tail gutter interference. Installation of the non-axisymmetric nozzle allows design options for trustvectoring and thrust reversing, the capabilities, which improve the manoeuvrability and handling of the aircraft[1,2].

* Current address: Dept. of Mechanical and Aerospace Engineering, Rutgers - The State University of New Jersey, NJ, 08855

The URS[3,4,5] (Upwind Relaxation Sweeping) algorithm suggested by the authors of this paper is employed for its efficiency and robustness to analyze the internal flow field of a nonaxisymmetric Transonic Nozzle.

Governing Equations

The 3D time-dependent, conservation of mass, Navier-Stokes and energy equations are the governing equations solved numerically in this paper. The nondimensional equations for compressible ideal gas in the absence of external forces, in conservation law form and in Cartesian coordinates are given below

$$\frac{\partial U}{\partial t}+\frac{\partial F}{\partial x}+\frac{\partial G}{\partial y}+\frac{\partial H}{\partial z}=\frac{1}{Re}\left[\frac{\partial R}{\partial x}+\frac{\partial S}{\partial y}+\frac{\partial T}{\partial z}\right] \quad (1)$$

where

$$U=\begin{bmatrix}\rho\\ \rho u\\ \rho v\\ \rho w\\ e\end{bmatrix}\quad F=\begin{bmatrix}\rho u\\ p+\rho u^2\\ \rho uv\\ \rho uw\\ (e+p)u\end{bmatrix}\quad G=\begin{bmatrix}\rho v\\ \rho uv\\ p+\rho v^2\\ \rho vw\\ (e+p)v\end{bmatrix}\quad H=\begin{bmatrix}\rho w\\ \rho uw\\ \rho vw\\ p+\rho w^2\\ (e+p)w\end{bmatrix} \quad (2)$$

$$R=\begin{bmatrix}0\\ \tau_{xx}\\ \tau_{xy}\\ \tau_{xz}\\ R_5\end{bmatrix}\quad S=\begin{bmatrix}0\\ \tau_{xy}\\ \tau_{yy}\\ \tau_{yz}\\ S_5\end{bmatrix}\quad T=\begin{bmatrix}0\\ \tau_{xz}\\ \tau_{yz}\\ \tau_{zz}\\ T_5\end{bmatrix} \quad (3)$$

$$\tau_{xx}=2/3\mu(2\frac{\partial u}{\partial x}-\frac{\partial v}{\partial y}-\frac{\partial w}{\partial z}) \tag{4}$$

$$\tau_{yy}=2/3\mu(2\frac{\partial v}{\partial y}-\frac{\partial u}{\partial x}-\frac{\partial w}{\partial z}) \tag{5}$$

$$\tau_{zz}=2/3\mu(2\frac{\partial w}{\partial z}-\frac{\partial u}{\partial x}-\frac{\partial v}{\partial y}) \tag{6}$$

$$\tau_{xy}=\tau_{yx}=\mu(\frac{\partial u}{\partial y}+\frac{\partial v}{\partial x}) \tag{7}$$

$$\tau_{xz}=\tau_{zx}=\mu(\frac{\partial w}{\partial x}+\frac{\partial u}{\partial z}) \tag{8}$$

$$\tau_{yz}=\tau_{zy}=\mu(\frac{\partial v}{\partial z}+\frac{\partial w}{\partial y}) \tag{9}$$

$$R_5=u\tau_{xx}+v\tau_{xy}+w\tau_{xz}+\frac{\mu}{(\gamma-1)Pr}\frac{\partial a^2}{\partial x} \tag{10}$$

$$S_5=u\tau_{xy}+v\tau_{yy}+w\tau_{yz}+\frac{\mu}{(\gamma-1)Pr}\frac{\partial a^2}{\partial y} \tag{11}$$

$$T_5=u\tau_{xz}+v\tau_{yz}+w\tau_{zz}+\frac{\mu}{(\gamma-1)Pr}\frac{\partial a^2}{\partial z} \tag{12}$$

The velocities are u, v, w, and e is the total energy per unit volume. The molecular viscosity μ is determined by the Sutherland law and Stokes hypothesis is used for the bulk viscosity $\lambda = -2\mu/3$. The Reynolds and Prandtl numbers are denoted as Re and Pr. Finally, the pressure p is determined by the ideal-gas law

$$p=(\gamma-1)[e - \rho(u^2 + v^2 + w^2)/2] \tag{13}$$

where γ is the ratio of specific heats, taken as $\gamma = 1.4$.

To discretize the equations using finite volume method, the equations should be written in the integral form. Let

$$R'=(F-\frac{\alpha}{Re}R)\cdot i_x+(G-\frac{\alpha}{Re}S)\cdot i_y+(H-\frac{\alpha}{Re}T)\cdot i_z \tag{14}$$

Using the Gauss theorem, the integral form of Eq. (1) is

$$\int_Q \frac{\partial U}{\partial t}dQ+\int_S R'\cdot ndS=0 \tag{15}$$

where Q is the volume bounded by the surface S and n is the outward pointing unit vector normal to the surface expressed as:

$$n = n_x i_x + n_y i_y + n_z i_z \tag{16}$$

The equations are discretized in the physical domain on the arbitrary body-fitted grid.
The flux crossing an interface of two adjacent cells is the normal component of vector R' given in Eq. (14). Let P_1 be the inviscid normal component of R_{inv} passing through unit interface.
where

$$R_{inv} = Fi_x + Gi_y + Hi_z \tag{17}$$

Thus

$$P_1= R_{inv}\cdot n = Fn_x + Gn_y + Hn_z$$

$$= U_n\begin{bmatrix}\rho\\ \rho u\\ \rho v\\ \rho w\\ e\end{bmatrix} + \begin{bmatrix}0\\ pn_x\\ pn_y\\ pn_z\\ pU_n\end{bmatrix} \tag{18}$$

where U_n is the normal component of the velocity expressed as:

$$U_n = un_x + vn_y + wn_z \qquad (19)$$

Van Leer's Flux Vector Splitting scheme is used to evaluate $\mathbf{P}_1$ at the volume interface[6,7].

URS Pprcedure

The concept of Upwind Relaxation-Sweeping is to select a direction with relatively smaller variable gradients as the global sweeping direction and to implement the local relaxation iteration on the control volume block in the main flow direction. The flow field is calculated by a series of global alternating outward/inward sweeps in the sweeping direction with the local forward/backward Gauss-Seidel iteration on each stream wise plane, one global sweep per time step. The global sweeping is also the time marching procedure.

Upwind differencing (Van Leer's FVS) is used for the convective and pressure terms and central differencing for the shear stress and heat flux terms. Third order MUSCL-type differencing[8] is used to evaluate the interface flux.

Suppose the sweeping direction is in z-direction with the index k increasing. Discretize the governing equations (15) nearly fully implicitly for the inviscid terms and explicitly for the viscous terms, we have:

$$\frac{U^{n+1}_{i,j,k}-U^{n}_{i,j,k}}{\Delta t}Q_{i,j,k} + (P^{+n+1}_{1_{i+\frac{1}{2},j,k}}+P^{-n+1}_{1_{i+\frac{1}{2},j,k}})\bullet S_{i+\frac{1}{2}}$$

$$+ (P^{+n+1}_{1_{i-\frac{1}{2},j,k}}+P^{-n+1}_{1_{i-\frac{1}{2},j,k}})\bullet S_{i-\frac{1}{2}}+(P^{+n+1}_{1_{i\,j+\frac{1}{2}\,k}}+P^{-n+1}_{1_{i\,j+\frac{1}{2}\,k}})\cdot S_{j+\frac{1}{2}}$$

$$+(P^{+n+1}_{1_{i\,j-\frac{1}{2}\,k}}+P^{-n+1}_{1_{i\,j-\frac{1}{2}\,k}})\cdot S_{j-\frac{1}{2}}+(P^{+n+1}_{1_{i\,j\,k+\frac{1}{2}}}+P^{-n}_{1_{i\,j\,k+\frac{1}{2}}})\cdot S_{k+\frac{1}{2}}$$

$$+(P^{+n\cdot 1}_{1_{i,j,k-\frac{1}{2}}}+P^{-n+1}_{1_{i,j,k-\frac{1}{2}}})\bullet S_{k-\frac{1}{2}} = RHS^{n}_{viscous} \qquad (20)$$

It is noted that $P^{-n}_{1_{i,j,k+\frac{1}{2}}}$ is discretized explicitly. To make the solution independent of the time step size, the implicit terms should be changed to Delta-form. To construct the implicit operator for Gauss-Seidel iteration, the Delta-form is only implemented for the terms with the same k index.

One implicit term left on the LHS is moved to RHS. Eq. (20) is then changed to:

$$[\frac{I}{\Delta t}Q+\sum\{(\frac{dP^+}{dU})_k+(\frac{dP^-}{dU})_k\}]\delta U^{n+1}=RHS^{n,n+1}_{inviscid}+RHS^{n}_{visco} \qquad (21)$$

where:
$\delta U^{n+1} = U^{n+1} - U^{n}$, $\Delta t^n = t^{n+1} - t^n$ and n is the iteration index,

$$RHS^{n,n+1}_{inviscid} = -\ [(P^{+n}_{1_{i+\frac{1}{2},j,k}} + P^{-n}_{1_{i+\frac{1}{2},j,k}})\bullet S_{i+\frac{1}{2}}$$

$$+ (P^{+n}_{1_{i-\frac{1}{2},j,k}}+P^{-n}_{1_{i-\frac{1}{2},j,k}})\bullet S_{i-\frac{1}{2}} +(P^{+n}_{1_{i\,j+\frac{1}{2}\,k}}+P^{-n}_{i_{i\,j+\frac{1}{2}\,k}})\cdot S_{j+\frac{1}{2}}$$

$$+ (P^{+n}_{1_{i\,j-\frac{1}{2}\,k}}+P^{-n}_{1_{i\,j-\frac{1}{2}\,k}})\cdot S_{j-\frac{1}{2}} +(P^{+n}_{1_{i\,j\,k+\frac{1}{2}}}+P^{-n}_{i_{i\,j\,k+\frac{1}{2}}})\cdot S_{k+\frac{1}{2}}$$

$$+ (P^{+n+1}_{1_{i,j,k-\frac{1}{2}}}+P^{n}_{1_{i,j,k-\frac{1}{2}}})\bullet S_{k-\frac{1}{2}}\ ] \qquad (22)$$

To keep the diagonal dominance and save computational work, first order differencing is used for the implicit terms and therefore the matrix M is penta-diagonal. The matrix equation for the cell (i,j,k) therefore can be written as:

$$B\delta U^{n+1}_{i,j+1,k} + A\delta U^{n+1}_{i,j,k} + C\delta U^{n+1}_{i,j-1,k} + E\delta U^{n+1}_{i-1,j,k}$$

$$+ D\delta U^{n+1}_{i+1\,j\,k} = RHS^{n,\,n+1}_{inviscid} + RHS^{n}_{viscous} \qquad (23)$$

where the coefficients A, B, C, D and E are 5x5 block matrices. The line Gauss-Seidel iteration is employed to inverse the matrix at the block composed of the cells with the same k index. Two sweeps are implemented at the local block k, one forward and the other backward. Implementation of only two sweep iterations is an approximation. After two local sweeps, the global iteration proceeds to the next block at k+1. The global sweeping starts with the inner solid wall with increasing k index. The variables are updated at each block soon after the two local sweeps for Gauss-Seidel iteration are completed. When the global iteration sweeps up to the outside solid wall, all the variables at time level n+1 are obtained and then the sweeping direction is reversed with decreasing k index to continue the iteration for the next time step. It is believed that the iteration with forward and backward sweeps at the local block, and outward and inward globally is beneficial for the information travelling through the entire flow field three-dimensionally and therefore rapidly. It is noted that $RHS^{n,\,n+1}_{inviscid}$ in Eq. (22) is not evaluated completely by using the variables at time level n and contains one term, $P^{+n+1}_{1_{i,j,k-\frac{1}{2}}}$, which is available due to the completion of the iteration at the k-1 block. When the global iteration sweeps in the direction with the decreasing k index , the explicit term in Eq. (20) is $P^{+n}_{1_{i,j,k-\frac{1}{2}}}$ instead of $P^{-n}_{1_{i\,j\,k+\frac{1}{2}}}$; the implicit term at time level n+1 in Eq. (22) is $P^{-n+1}_{1_{i\,j\,k+\frac{1}{2}}}$ instead of $P^{+n+1}_{1_{i\,j\,k-\frac{1}{2}}}$. Supposing each interface sub-flux has the same weight, the URS method is thus 11/12 implicit and 1/12 explicit. The URS algorithm is proven to be unconditionally stable. The gain from the 1/12 explicit discretization is significant: 1) the Jacobians and δU^{n+1} are only stored in one plane on which Gauss-Seidel iteration is implemented and therefore the whole storage is greatly reduced; 2) only one global sweep per time step is needed to solve all the unknowns in a time level and therefore the CPU time per time step is saved.

The accuracy of the converged solution is controlled by RHS. Even though the inviscid terms are evaluated by using third order accuracy, the general accuracy of the solution for the 3D Navier-Stokes equations is second order since central differencing is used for the viscous terms.

Results

To test the accuracy of the computer code, the flat plat Blasius problem is solved first with Reynolds number 10000 at Mach number equal to 0.3. The grid is 101x51 and the cell Reynolds number 0.18 for the first grid on the wall and 2.0 for the second grid. The velocity profile and surface friction coefficient agree well with the analytical solution as shown in Fig. 1.

Figure 2 is the half geometry of the nozzle with the grid size of 101x31x51. Only the half nozzle is calculated due to the symmetry of the geometry. Figure 3 presents the Mach number contours of the flow field at different locations in z-direction. In the middle plane (Z/L=0.0), there is an oblique shock wave right after the throat. The shock wave are weak because the Mach number is only slightly greater than one after the throat. The two shock waves extending from the lower and upper wall intersect at the center-line of the nozzle and then reach the wall of the other side. After approaching the wall, the oblique shock waves reflect. These reflections intersect and reflect again until the flow approaches the exit of the nozzle. It can be seen from Fig. 3 that the intensity of the shock waves becomes weaker with repeated intersections and reflections. This can be also quantitatively seen from the pressure distributions given in Fig. 4. Fig. 4 (a), (b), (c) are at the bottom wall with different locations from the center-line (Z/L=0.) to the one near the side wall (Z/L=0.875). Fig.4 (d) is the pressure distribution along the side wall center-line. Most of the computational points agree very well with the experiment[9] except the point at the first shock reflection. The first reflection calculated seems to be not strong enough. Finer grid may be needed to obtain the better resolution of the reflection. The flow fields are highly three-dimensional in the vicinities of the corners due to the boundary layer interaction between the side walls and the lower or upper walls, particularly after the throat, where the main flow is supersonic. Fig. 5 shows the spanwise section velocity vector fields for nozzle A1. Fig. 5 indicates that there is very weak secondary flow before the throat where the flow is subsonic and the secondary flow becomes much stronger after the throat where the flow is supersonic. Fig. 5 (b), (c) , (d) and (e) show that the cross velocity vector fields are different at different locations. The cross flow is at the corners for Fig. 5 (b) where the oblique shock wave after the throat just grows up. Fig. 5 (c) shows that there exist cross flow near the center plane in y-direction. It is made by the shock wave and side wall boundary layers interactions, where the shocks from lower and upper wall intersect. After the shock intersection, the cross flow is again concentrated in the corners as shown in Fig. 5 (d).

The maximum CFL number used reaches the order of 10^7. Rapid convergence rate has been obtained. Four magnitude order of the residual is reduced by using less than 200 iterations.

Conclusion

The viscous flow field of a three-dimensional non-axisymmetric transonic nozzle is numerically analyzed. URS algorithm is employed to solve the 3D Navier-Stoke equations. Oblique shock waves and reflections are captured with the interaction with the wall boundary layers. There is strong secondary flow after the throat in the supersonic region in the corner of the side and bottom walls due to the shock wave/boundary layer interaction. The computed pressure distributions agree well with the experiment.

References

1. Maiden, Donald L. and Berrier, Bobby L., " Effect of Airframe Modifications on Longitudinal Aerodynamic Characteristics of a Fixed-Wing, Twin- Jet Fighter Airplane Model", NASA TM X-2523, 1972

2. Maiden, Donald L. and Petit, John E, " Investigation of Two-Dimensional Wedge Exhaust Nozzles for Advanced Aircraft", Journal of Aircraft, Vol.13, No.10, 1976

3. Zha,G.C. and Bilgen, E., " An Efficient Upwind Relaxation-Sweeping Algorithm for Three-Dimensional Navier-Stokes Equations" AIAA Paper 92-0023, 1992

4. Zha,G.C, and Bilgen, E., " Nnmerical Simulation of Three-Dimensional Inviscid Internal Flows Using Unfactored Upwind-Relaxation Sweeping Algorithm " AIAA Paper 94-0396, 1994

5. Zha, G.C., " Numerical Solutions of Three-Dimensional Transonic Flows Based on Upwind Schemes", Ph.D. Thesis, Ecole Polytechnique, University of Montreal, March 1994.

6. Van Leer, B., " Flux-vector splitting for the Euler equations", Lecture Note in Physics, Vol. 170, 1982

7. Zha,G.C. and Liu, D.Z., " An Efficient Upwind Relaxation-Sweeping Algorithm for Three-Dimensional Euler Equations", AIAA Paper 90-0129, 1990

8. Van Leer,B., Thomas, J.L., Roe, P.L. and Newsome, R.W, " A Comparison of Numerical Flux Formulas for the Euler and Navier-Stokes Equations", AIAA Paper 87-1104, 1987

9. Mason, Mary L., Putnam, Lawrence E. and Re, Richard J., " The Effect of Throat Contouring on Two-Dimensional Converging-Diverging Nozzles at Static Conditions", NASA TP-1704, 1980

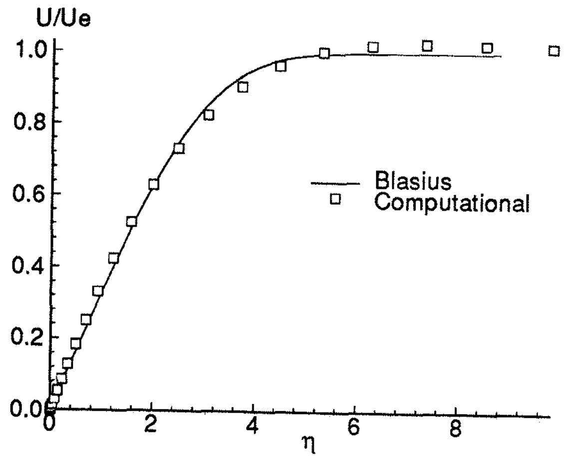

Velocity Profiles

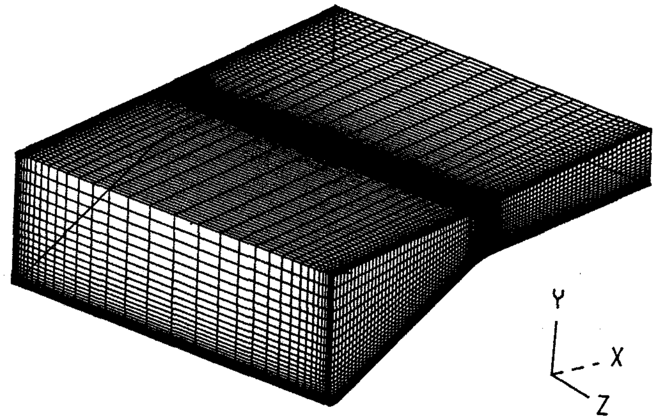

Fig2. The Geometry and Grid of the Nozzle

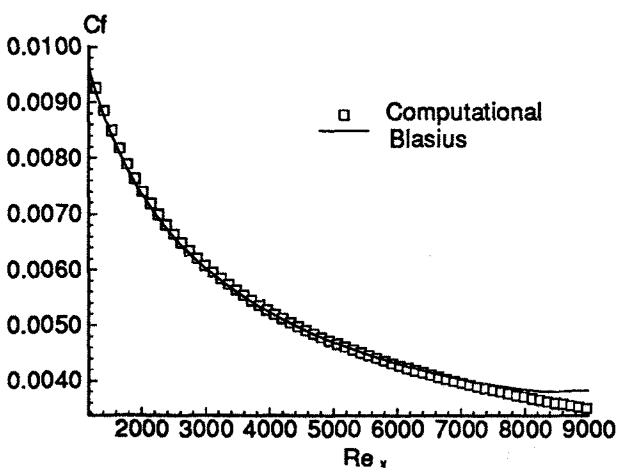

Friction Coefficient Distributions

Fig. 1 Results for Blasius Flow

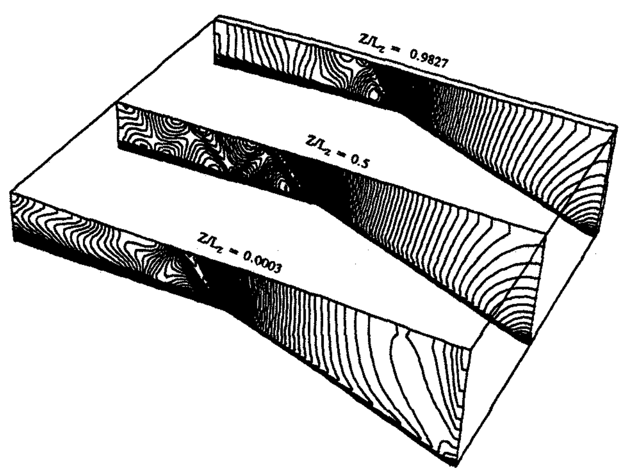

Fig. 3 Mach Number Contours of the Nozzle

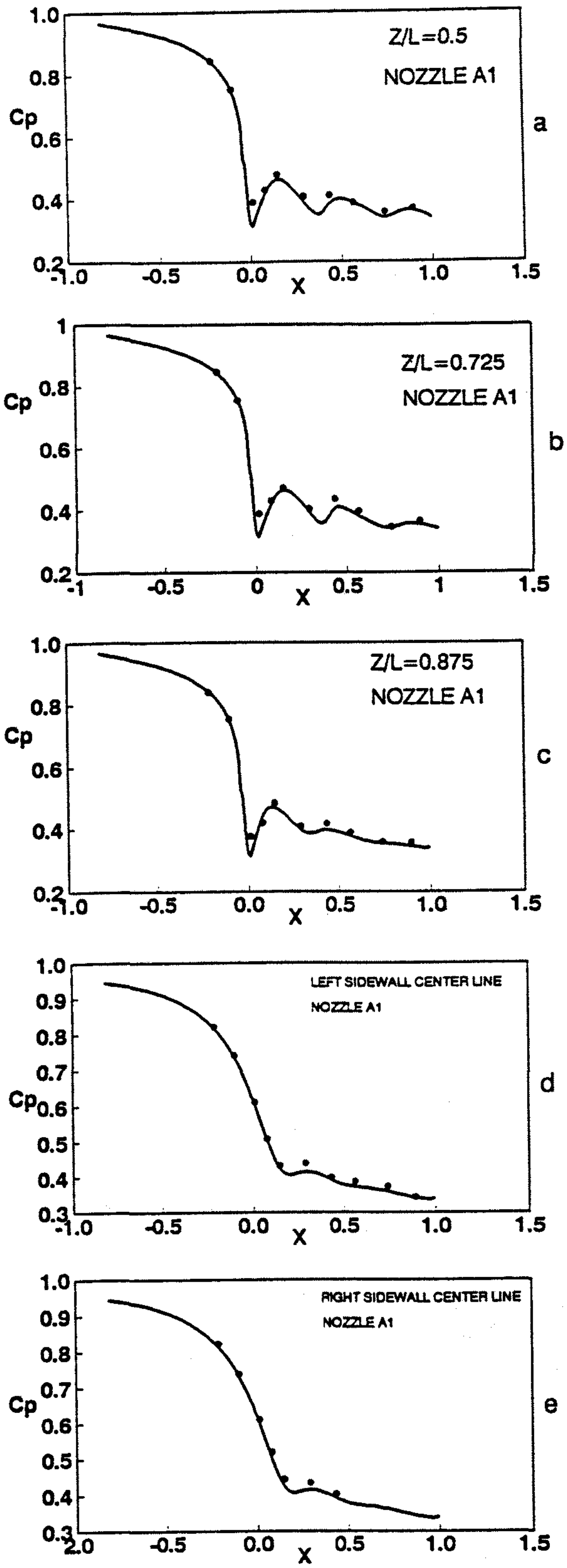

Fig.4 Pressure Distributions of the Nozzle
• Experiment, – Calculation

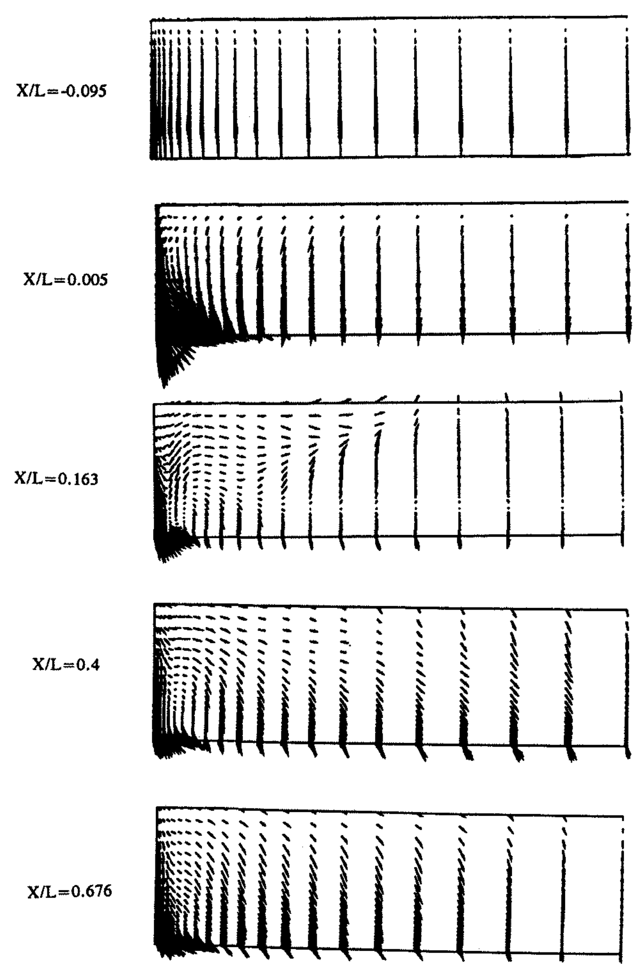

Fig. 5 Spanwise Velocity Fields at Different Locations